Available online at www.sciencedirect.com
ScienceDirect
Journal of Sound and Vibration 318 (2008) 1291–1312
JOURNAL OF SOUND AND VIBRATION
www.elsevier.com/locate/jsvi

A hydroelastic investigation of circular cylindrical shells-containing flowing fluid with different end conditions ☆

B. Uğurlu, A. Ergin*

Faculty of Naval Architecture and Ocean Engineering, Istanbul Technical University, Maslak, 34469 Istanbul, Turkey

Received 16 January 2007; received in revised form 25 March 2008; accepted 8 May 2008
Handling Editor: A.V. Metrikine
Available online 24 June 2008

Abstract

This paper presents the effects of different end conditions on the response behavior of thin circular cylindrical shell structures fully in contact with flowing fluid. The investigated end conditions are as follows: simply supported, clamped–clamped, clamped–simply supported and clamped–free (cantilever shell) ends. Additionally, the dynamic responses of a tapered cylindrical shell conveying flowing fluid and simply supported at its ends were investigated. The method employed in this study is a hybrid method—a boundary integral equation method for the calculation of the fluid–structure interaction effects and a finite element method for the structural analysis. In this study, the mathematical model presented before [B. Uğurlu, A. Ergin, A hydroelasticity method for vibrating structures containing and/or submerged in flowing fluid, *Journal of Sound and Vibration* 290 (2006) 572–596] is extended by applying the direct boundary integral equation method, and by using a higher-order panel method (linear distribution). It should also be said that the method used in this study could be applied to any shape of cylindrical structure in contact with internal and/or external flowing fluid, in contrast to the studies found in the literature. In the analysis of the linear fluid–structure system, it is assumed that the fluid is ideal, i.e., inviscid, incompressible and its motion is irrotational. It is assumed that the flexible structure vibrates in its *in-vacuo* modes when it is in contact with flowing fluid, and that each mode gives rise to a corresponding surface pressure distribution on the wetted surface of the structure. The *in-vacuo* dynamic properties of the dry structure are obtained by using a standard finite element software. In the wet part of the analysis, the wetted surface is idealized by using appropriate boundary elements, referred to as hydrodynamic panels. The fluid–structure interaction forces are calculated in terms of the generalized added mass coefficients, generalized Coriolis fluid force coefficients and generalized centrifugal fluid force coefficients. To demonstrate the applicability of the method and assess the influences of the flowing fluid and end support conditions on the dynamic response behavior of the shell structures, the non-dimensional eigenfrequencies and associated eigenmodes are presented as a function of the non-dimensional axial flow velocity, and they compare well with the analytical solutions found in the literature.

☆This paper is devoted to Professor W.G. Price on his retirement from Southampton University.

*Corresponding author. Tel.: +90 212 2856414; fax: +90 212 2856454.
E-mail address: ergina@itu.edu.tr (A. Ergin).

0022-460X/$ - see front matter © 2008 Elsevier Ltd. All rights reserved.
doi:10.1016/j.jsv.2008.05.006

1. Introduction

Cylindrical structures are widely used in engineering practice for conveying flowing fluid, or for other purposes. For instance, a fluid conveying piping system may be modeled as a circular cylindrical shell subjected to axial flow and periodically supported. A large extent of a submarine pressure hull may also be considered as a cylindrical shell structure in contact with an external flowing fluid medium, due to the forward velocity of the submarine. Furthermore, the circular cylindrical shell idealization may also be used for heat exchanger tubes in axial flow. In all these engineering applications, the dynamic interaction between the structure and fluid medium (axial flow) plays an important role on the response behavior of the shell structures. This is due to the vibration of the structural surface in contact with the fluid medium imparting motion to the fluid (flow), thus altering its pressure, and, hence inducing reactive forces on its surface.

The dynamic response behavior of circular cylindrical shells immersed in or conveying flowing fluid has been extensively studied, and general reviews of the literature have been given by Païdoussis [1] and Païdoussis and Li [2]. Also, relatively recent books by Païdoussis [3,4] provide a comprehensive treatment of the subject as well as a complete bibliography of all-important work in the field.

For the interaction problems involving structures of simple shapes such as cylindrical shells subjected to axial flow, approximate analytical solutions are available. For instance, Amabili and Garziera [5] presented a study on the linear dynamic analysis of cylindrical shells with flowing fluid. They investigated the influence of various complicating effects, such as non-uniform edge boundaries; internal, external and annular flows; intermediate constraints, etc., on the dynamic response behavior of the structure. On the other hand, a three-part study, investigating the dynamics of cantilever cylinders in axial flow, has been reported. In the first part, Païdoussis et al. [6] presented some old and new experimental results, and a comparison with linear theory was made. In the second part [7], a weakly nonlinear equation of motion was derived. The fluid dynamic forces were introduced in terms of virtual work expressions, separately for the inviscid forces, and for the hydrostatic and frictional forces. The results of calculations based on this theoretical model were presented in Part three [8], by means of bifurcation diagrams, phase-plane plots and Poincaré maps. Amabili et al. [9] developed a geometrically nonlinear shell model to study stability of shells-containing incompressible flow. However, the fluid–structure interaction forces were calculated by using a linear potential theory. This study was further extended by Amabili et al. [10], for investigating the nonlinear stability of supported, circular cylindrical shells in a compressible, inviscid, subsonic flow. In an investigation by Amabili et al. [11], the nonlinear dynamics and stability of simply supported, circular cylindrical shells-containing inviscid, incompressible fluid flow were studied. The linear potential flow theory was again applied to describe the fluid–structure interaction forces. On the other hand, Langthjem and Olhoff [12] employed the separation of variables and Galerkin methods for discretization of the equations of motion for a cantilevered cylindrical fluid conveying shell. In this study, the perturbation velocity potential function was expressed in terms of a series of orthonormal beam modal functions. Recently, Karagiozis et al. [13] performed an experimental study on the nonlinear dynamics and stability characteristics of thin-walled, clamped–clamped circular cylindrical shells in contact with flowing fluid. The experiments were carried out for three different test set-ups: elastomer shells in annular airflow, elastomer shells with internal airflow, and aluminum or plastic shells with internal water flow. In all the test cases, the cylindrical shell structures lost their stabilities in the form of divergence at sufficiently high flow velocities.

Very recently, Uğurlu and Ergin [14] presented a general three-dimensional hydroelasticity method for investigating the dynamics of elastic structures containing and submerged in flowing fluid. The method is a combined finite element (FE)–boundary element (BE) procedure utilizing a boundary integral formulation for the potential fluid problem. In order to demonstrate the applicability of the method, they adopted a circular cylindrical shell simply supported at both ends for the calculations.

The FE method has also been widely applied to investigate the linear and nonlinear dynamic response behavior of shell structures. For instance, Lakis and Selmane [15] presents a hybrid FE method to investigate the large amplitude vibrations of orthotropic cylindrical shells subjected to flowing fluid. In this study, only the linear effects of the fluid were taken into account. Toorani and Lakis [16,17] presented a method, based on the FE method, refined shell theories and linear fluid dynamic theory, to analyze the vibration of anisotropic laminated composite cylindrical shells subjected to internal and external incompressible, inviscid flowing fluid.

Furthermore, Toorani and Lakis [18] used the same method and presented the fluid-induced vibration characteristics of the anisotropic laminated cylindrical shells partially or completely filled with a quiescent liquid or subjected to a flowing fluid. On the other hand, Zhang et al. [19,20] proposed a FE formulation to predict the dynamic response behavior of cylindrical shells conveying quiescent or flowing fluid. The method presented is based on the three-dimensional theory of elasticity and the linearized Eulerian equations. The effects of the end support conditions (simply supported, clamped–clamped and clamped–free ends) on the response behavior were also investigated.

In this paper, the effects of the end support conditions on the response behavior of thin cylindrical shell structures in contact with flowing fluid are presented. The investigated end support conditions are as follows: simply supported, clamped–clamped, clamped–simply supported, clamped–free (cantilever shells) ends. Furthermore, a tapered cylindrical shell conveying flowing fluid and simply supported at its ends was also adopted for the calculations, and its *wet* non-dimensional frequencies were predicted as a function of the non-dimensional axial flow velocity. The method employed in this study is based on a boundary integral equation method, and it is already successfully applied to a circular cylindrical shell with simply supported ends (see Ref. [14]). In this study, the mathematical model is extended by applying the direct boundary integral equation method, instead of the indirect approach used in Ref. [14]. Furthermore, on the contrary to the previous study [14] in which a constant source distribution was assumed over each hydrodynamic panel, a higher-order panel method (linear distribution) is adopted in the present study in order to obtain a better approximation and achieve a faster convergence for the hydrodynamic properties. It should also be said that the method used in this study could be applied to any shape of cylindrical structure in contact with internal and/or external flowing fluid, in contrast to the studies found in the literature.

For the simply supported end conditions, a cylindrical shell with rigid and flexible extensions, respectively, was considered. The cylindrical shell with rigid extensions corresponds to a finite length, flexible cylindrical shell connected to infinitely long rigid cylindrical baffles, of the same diameter as the shell, at both ends. However, the cylindrical shell with flexible extensions coincides with one that is infinitely long and periodically supported.

In this study, it is assumed that the fluid is ideal, i.e., inviscid, incompressible and its motion is irrotational. It should be noted that both steady and unsteady viscous effects are neglected (see, for instance, Ref. [21]). It is also assumed that the flexible shell structure vibrates in its *in-vacuo* eigenmodes when it is in contact with flowing fluid, and that each mode gives rise to a corresponding surface pressure distribution on the wetted surface of the structure. The *in-vacuo* dynamic analysis entails the vibration of the shell in the absence of any external force and structural damping, and the corresponding dynamic characteristics (e.g., natural frequencies and mode shapes) of the shell structures were obtained by using a standard FE software (i.e., Ref. [22]).

At the fluid–structure interface, continuity considerations require that the normal velocity of the fluid is equal to that of the structure. The normal velocities on the wetted surface are expressed in terms of modal structural displacements and their derivatives, with respect to the x-coordinate (see Fig. 1), obtained from the *in-vacuo* dynamic analysis. By using a boundary integral equation method the fluid pressure is eliminated from the problem, and the fluid–structure interaction forces are calculated in terms of the generalized hydrodynamic

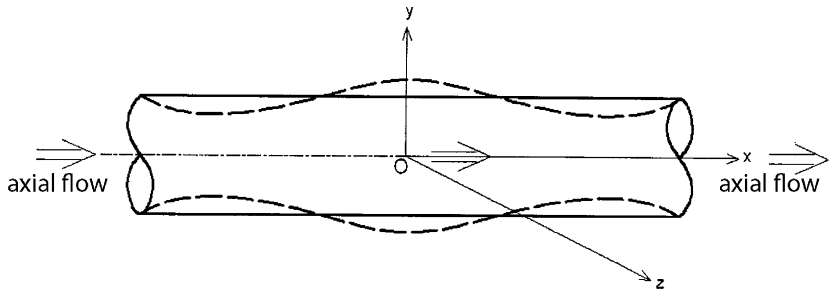

Fig. 1. Cylindrical shell conveying flowing fluid.

added mass coefficients (due to the inertia effect of fluid), generalized fluid-damping coefficients (due to the Coriolis acceleration of fluid) and generalized fluid stiffness coefficients (due to the centrifugal effect of fluid).

During the analysis, the wetted surface was idealized by using appropriate BEs, referred to as hydrodynamic panels. The generalized mass matrix was merged with the generalized hydrodynamic added mass matrix, and the generalized structural stiffness matrix with the generalized fluid stiffness matrix. Then, the total generalized mass and stiffness matrices were used together with the generalized fluid-damping matrix in solving the eigenvalue problem for the shell structure containing flowing fluid. To assess the influences of flowing fluid and end support conditions on the response behavior of the shell structures, the non-dimensional eigenfrequencies and mode shapes are presented as a function of the non-dimensional flow velocity. The predictions based on the method used were compared with those results found in the open literature, and a very good comparison is obtained between the results.

2. Mathematical model

2.1. Fluid–structure interaction problem

The fluid is assumed ideal, i.e., inviscid and incompressible, and its motion is irrotational and there exists a fluid velocity vector, $\mathbf{v}$, which can be defined as the gradient of the velocity potential function Φ as

$$\mathbf{v}(x,y,z,t) = \nabla\Phi(x,y,z,t). \tag{1}$$

The velocity potential Φ may be expressed as

$$\Phi = Ux + \phi. \tag{2}$$

Here the steady velocity potential Ux represents the effect of the mean flow associated with the undisturbed flow velocity U in the axial direction. Further, ϕ is the unsteady velocity potential associated with the perturbations to the flow field due to the motion of the flexible body, and satisfies the Laplace equation

$$\nabla^2\phi = 0, \tag{3}$$

throughout the fluid domain.

For the structure containing flowing fluid, the vibratory response of the structure may be expressed in terms of principal coordinates as [23,24]

$$\mathbf{p}(t) = \mathbf{p}_0\, e^{\lambda t}, \tag{4}$$

where $\mathbf{p}_0$ represents the complex response amplitude vector and λ is complex non-zero constant, and t is the time. The imaginary part of λ is the circular frequency of oscillations and its real part gives an exponential growth or decay. The velocity potential function due to the distortion of the structure in the rth *in-vacuo* vibrational mode may be written as follows:

$$\phi_r(x,y,z,t) = \phi_r(x,y,z)p_{0r}\, e^{\lambda t}, \quad r = 1,2,\ldots,M, \tag{5}$$

where M represents the number of modes of interest, and p_{0r} is an unknown complex amplitude for the rth principal coordinate.

On the wetted surface of the vibrating structure the normal fluid velocity must equal to the normal velocity on the structure, and this condition for the rth modal vibration of the elastic structure containing flowing fluid can be expressed as

$$\frac{\partial\phi_r(x,y,z,t)}{\partial n} = \left(\frac{\partial\mathbf{u}_r(x,y,z,t)}{\partial t} + U\frac{\partial\mathbf{u}_r(x,y,z,t)}{\partial x}\right)\cdot\mathbf{n}, \tag{6}$$

where $\mathbf{n}$ is the unit normal vector on the wetted surface and points out of the domain. The vector $\mathbf{u}_r$ denotes the displacement response of the structure in the rth principal coordinate and it may be written as

$$\mathbf{u}_r(x,y,z,t) = \mathbf{u}_r(x,y,z)p_{0r}\, e^{\lambda t} \tag{7}$$

where $\mathbf{u}_r\,(x,y,z)$ is the rth modal displacement vector of the median surface of the structure, and it is obtained from the *in-vacuo* analysis.

Substituting Eqs. (5) and (7) into Eq. (6), the following expression is obtained for the boundary condition on the fluid–structure interface:

$$\frac{\partial \phi_r(x,y,z)}{\partial n} = \lambda \mathbf{u}_r(x,y,z)\cdot\mathbf{n} + U\frac{\partial \mathbf{u}_r(x,y,z)}{\partial x}\cdot\mathbf{n}. \tag{8}$$

It should be noted that, for the completely filled elastic structure, the normal fluid velocity could not be arbitrarily specified. It has to satisfy the incompressibility condition [25]

$$\iint_{S_W} \frac{\partial \phi_r}{\partial n}\,\mathrm{d}S = 0, \tag{9}$$

where S_W represents the wetted surface of the elastic structure.

2.2. Numerical evaluation of perturbation potential ϕ

The boundary value problem for the perturbation potential, ϕ, may be expressed in the following boundary integral equation form (see, for example, Refs. [25–27]):

$$c(\xi)\phi(\xi) = \iint_{S_W} (\phi^*(s,\xi)q(s) - \phi(s)q^*(s,\xi))\,\mathrm{d}S, \tag{10}$$

where ξ and s denote, respectively, the source and field points on the wetted surface. ϕ^* is the fundamental solution and expressed as follows:

$$\phi^*(s,\xi) = \frac{1}{4\pi r}. \tag{11}$$

$q = \partial\phi/\partial n$ is the flux (on the fluid–structure interface, it represent the fluid velocities normal to the wetted structural surface), and r the distance between the source and field points. The free term $c(\xi)$ is defined as the fraction of $\phi(\xi)$ that lies inside the domain of interest [26]. Moreover, $q^*(s,\xi)$ can be written as

$$q^*(s,\xi) = -(\partial r/\partial n)/4\pi r^2 \tag{12}$$

The fluid–structure interaction problem may be separated into two parts as in Uğurlu and Ergin [14]: (i) the vibration of elastic structure in a quiescent fluid, and (ii) the disturbance in the main axial flow due to the oscillation of structure. Thus, defining $\phi = \lambda\phi_1 + U\phi_2$, Eq. (8) may be divided into two separate parts as

$$\frac{\partial \phi_1}{\partial n} = \mathbf{u}(x,y,z)\cdot\mathbf{n}, \tag{13a}$$

$$\frac{\partial \phi_2}{\partial n} = \frac{\partial \mathbf{u}(x,y,z)}{\partial x}\cdot\mathbf{n}, \tag{13b}$$

where ϕ_1 represents the displacement potential due to the vibration of the structure in a quiescent fluid, and ϕ_2 denotes the disturbing effect of the term $\partial u/\partial x$ to the main axial flow field. $\mathbf{u}$ is the *in-vacuo* modal displacement vector.

For the solution of Eq. (10) with boundary conditions (13a) and (13b), the wetted surface can be idealized by using BEs, referred to as hydrodynamic panels, and the distribution of the potential function and its flux over each hydrodynamic panel may be described in terms of the shape functions and nodal values as

$$\phi_e = \sum_{j=1}^{n_e} N_{ej}\phi_{ej}, \quad q_e = \sum_{j=1}^{n_e} N_{ej}q_{ej} \tag{14}$$

Here, n_e represents the number of nodal points assigned to the eth hydrodynamic panel, and N_{ej} the shape function adopted for the distribution of the potential function. For a quadrilateral panel having four nodal

points at its corners, n_e takes on the value of 4. e represents the eth hydrodynamic panel. In the case of a linear distribution adopted in this study, the shape functions for the eth quadrilateral panel may be expressed as (see Ref. [26])

$$\begin{aligned} N_{e1} &= ((1-\zeta)(1-\eta))/4, \\ N_{e2} &= ((1+\zeta)(1-\eta))/4, \\ N_{e3} &= ((1+\zeta)(1+\eta))/4, \\ N_{e4} &= ((1-\zeta)(1+\eta))/4 \end{aligned} \tag{15}$$

in the local coordinate system—$\zeta\eta$ of the eth panel.

After substituting Eqs. (14) and (15) into Eq. (10) and applying the boundary conditions given in Eqs. (13a) and (13b), the unknown nodal potential function values can be determined from the following sets of algebraic equations [27]

$$c_k\phi_{1k} + \sum_{i=1}^{M_p}\sum_{j=1}^{n_i}(\phi_{1ij}\iint_{\Delta S_i} N_j q^* \,\mathrm{d}S = \sum_{i=1}^{M_p}\sum_{j=1}^{n_i}(\mathbf{u}_{ij}\cdot\mathbf{n}_j \iint_{\Delta S_i} N_j\phi^* \,\mathrm{d}S), \quad k = 1,2,\ldots,n_p, \tag{16a}$$

$$c_k\phi_{2k} + \sum_{i=1}^{M_p}\sum_{j=1}^{n_i}(\phi_{2ij}\iint_{\Delta S_i} N_j q^* \,\mathrm{d}S = \sum_{i=1}^{M_p}\sum_{j=1}^{n_i}\left(\frac{\partial \mathbf{u}_{ij}}{\partial x}\cdot\mathbf{n}_j \iint_{\Delta S_i} N_j\phi^* \,\mathrm{d}S\right), \quad k = 1,2,\ldots,n_p, \tag{16b}$$

where n_p and n_i denote the number of nodal points used in the discretization of the structure and number of nodes assigned to the ith panel, respectively. M_p is the number of hydrodynamic panels used in the discretization. ϕ_{1ij} (and ϕ_{2ij}) and $\mathbf{u}_{ij}$ represent, respectively, the potential and displacement vector for the jth nodal point of the ith hydrodynamic panel.

2.3. Calculation of generalized fluid–structure interaction force coefficients

Using the Bernoulli's equation and neglecting the second-order terms, the dynamic fluid pressure on the elastic structure due to the rth modal vibration becomes

$$P_r(x,y,z,t) = -\rho_f\left(\frac{\partial\phi_r}{\partial t} + U\frac{\partial\phi_r}{\partial x}\right), \tag{17}$$

where ρ_f is the fluid density. Substituting Eq. (5) into Eq. (17), the following expression for the pressure is obtained:

$$P_r(x,y,z,t) = -\rho_f\left(\lambda\phi_r + U\frac{\partial\phi_r}{\partial x}\right)p_{0r}\,\mathrm{e}^{\lambda t}. \tag{18}$$

By using the definition of $\phi_r = \lambda\phi_{r1} + U\phi_{r2}$, Eq. (18) may be rewritten in the following form:

$$P_r(x,y,z,t) = -\rho_f\left(\lambda^2\phi_{r1} + U\lambda\left(\frac{\partial\phi_{r1}}{\partial x} + \phi_{r2}\right) + U^2\frac{\partial\phi_{r2}}{\partial x}\right)p_{0r}\,\mathrm{e}^{\lambda t}. \tag{19}$$

The kth component of the generalized fluid–structure interaction force due to the rth modal *in-vacuo* vibration of the elastic structure subjected to axial flow can be expressed in terms of the pressure acting on the

wetted surface of the structure as

$$\begin{aligned} Z_{kr} &= \iint_{S_W} P_r(x,y,z,t)\mathbf{u}_k\mathbf{n}\,\mathrm{d}S \\ &= -p_{0r}\,\mathrm{e}^{\lambda t}\iint_{S_W}\rho_f\left(\lambda^2\phi_{r1}+U\lambda\left(\frac{\partial\phi_{r1}}{\partial x}+\phi_{r2}\right)+U^2\frac{\partial\phi_{r2}}{\partial x}\right)\mathbf{u}_k\mathbf{n}\,\mathrm{d}S \\ &= -\lambda^2 p_{0r}\,\mathrm{e}^{\lambda t}\rho_f\iint_{S_W}\phi_{r1}\mathbf{u}_k\mathbf{n}\,\mathrm{d}S-\lambda p_{0r}\,\mathrm{e}^{\lambda t}\rho_f U\iint_{S_W}\left(\frac{\partial\phi_{r1}}{\partial x}+\phi_{r2}\right)\mathbf{u}_k\mathbf{n}\,\mathrm{d}S \\ &\quad -p_{0r}\,\mathrm{e}^{\lambda t}\rho_f U^2\iint_{S_W}\frac{\partial\phi_{r2}}{\partial x}\mathbf{u}_k\mathbf{n}\,\mathrm{d}S \end{aligned} \tag{20}$$

The generalized added mass, A_{kr}, generalized fluid damping (due to the Coriolis acceleration of fluid), B_{kr} and generalized fluid stiffness (due to the centrifugal effect of fluid), C_{kr} terms can be defined as

$$A_{kr}=\rho_f\iint_{S_W}\phi_{r1}\mathbf{u}_k\mathbf{n}\,\mathrm{d}S, \tag{21}$$

$$B_{kr}=\rho_f U\iint_{S_W}\left(\frac{\partial\phi_{r1}}{\partial x}+\phi_{r2}\right)\mathbf{u}_k\mathbf{n}\,\mathrm{d}S, \tag{22}$$

$$C_{kr}=\rho_f U^2\iint_{S_W}\frac{\partial\phi_{r2}}{\partial x}\mathbf{u}_k\mathbf{n}\,\mathrm{d}S. \tag{23}$$

Therefore, the generalized fluid–structure interaction force component, Z_{kr}, can be written as

$$\begin{aligned} Z_{kr}(t) &= -A_{kr}\lambda^2 p_{0r}\,\mathrm{e}^{\lambda t}-B_{kr}\lambda p_{0r}\,\mathrm{e}^{\lambda t}-C_{kr}p_{0r}\,\mathrm{e}^{\lambda t} \\ &= -A_{kr}\ddot{p}_r(t)-B_{kr}\dot{p}_r(t)-C_{kr}p_r(t). \end{aligned} \tag{24}$$

2.4. Calculation of wet frequencies and mode shapes

The generalized equation of motion for the elastic structure in contact with axial flow assuming free vibrations with no structural damping is

$$\left[\lambda^2(\mathbf{a}+\mathbf{A})+\lambda(\mathbf{B})+(\mathbf{c}+\mathbf{C})\right]\mathbf{p}=0, \tag{25}$$

where **a** and **c** denote the generalized structural mass and stiffness matrices, respectively, and they are calculated by using a standard FE program [22]. The matrices **A**, **B** and **C** represent the generalized added mass, generalized fluid damping and generalized fluid stiffness matrices, respectively.

It should be noticed that the eigenvalue λ is generally complex. It was observed from the solution of the eigenvalue problem that, before the onset of the instability, the eigenvalues (wet frequencies) have zero real parts for a conservative fluid–structure interaction system. On the other hand, the eigenvectors **p** have both real and imaginary parts, which are generally different from zero. Therefore, the eigenvectors (modes) are complex. However, when the axial mean flow velocity is zero, the eigenvectors only have real parts.

3. Numerical results and comparisons

A group of calculations have been performed in order to demonstrate the applicability of the aforementioned theory to structures containing flowing fluid. The dynamics and stability of fluid conveying cylindrical shells having separately simply supported, clamped–clamped, simply supported–clamped and

clamped–free (cantilever cylinder) end conditions were investigated, and the calculations were compared with the results found in the open literature. Furthermore, a tapered cylindrical shell conveying flowing fluid and simply supported at its ends was also adopted for the calculations.

A right-handed Cartesian coordinate system, xyz, is adopted in the present study, and it is shown in Fig. 1 for a cylindrical shell subjected to flow. The coordinate system is fixed in space with its origin at O. The x-axis lies along the length L, and coincides with the centerline of the cylindrical shell.

The mode shapes of cylindrical shells in vacuum are identified with the number of standing waves around the circumference, n, and the number of half-waves along the shell, m. A combination of m and n forms a particular mode shape (m, n). The mode shapes occur in pairs. That is, in general, for each natural frequency, there exists a pair of mode shapes satisfying the relevant orthogonality conditions.

For convenience, the following non-dimensional parameters are introduced as in Weaver and Unny [28]:

$$V = U/\left\{(\pi^2/L)\left[D/(\rho_s h)\right]^{1/2}\right\}, \quad \Omega = \lambda/\left\{(\pi^2/L^2)\left[D/(\rho_s h)\right]^{1/2}\right\}. \tag{26}$$

Here, V and Ω denote the non-dimensional axial fluid velocity and non-dimensional eigenfrequency, respectively, and λ is the corresponding complex eigenvalues of the cylindrical shell conveying flowing fluid. h and ρ_s represent, respectively, the thickness and density of the shell structure. Furthermore, D is the flexural rigidity, and it is defined as $D = Eh^3/12(1-\nu^2)$. E and ν denote, respectively, Young's modulus and Poisson's ratio.

3.1. Cylindrical shell with simply supported ends

The structure adopted for calculations is a finite length cylindrical shell, simply supported at both ends, and it was analytically investigated by Weaver and Unny [28], Selmane and Lakis [29], Amabili et al. [9] and Amabili and Garziera [5]. The shell structure has the geometric and material properties: length-to-radius ratio $L/R = 2$, thickness-to-radius ratio $h/R = 0.01$, Young's modulus $E = 206\,\text{GPa}$, Poisson's ratio $\nu = 0.3$, and mass density $\rho_s = 7850\,\text{kg/m}^3$. Fresh water is used as the contained fluid with a density of $\rho_f = 1000\,\text{kg/m}^3$.

The *in-vacuo* dynamic properties of this simply supported shell were obtained using the ANSYS FE software [22]. This produces information on natural frequencies and normal mode shapes of the *dry* structure in vacuum. In these FE calculations, the cylindrical shell was discretized with four-noded quadrilateral shell elements, including both membrane and bending stiffness influences. A FE convergence test study was performed in order to obtain the converged *in-vacuo* dynamic properties (natural frequencies, mode shapes). For this purpose, four different idealizations were considered: 1152, 2048, 3200 and 4800 FEs distributions over the shell structure. In the first idealization with 1152 four-noded quadrilateral FEs, 48 and 24 elements, respectively, were distributed around the circumference and along the shell structure. To test the convergence, the number of elements around the circumference and along the shell was, first, increased to 64 and 32, and then to 80 and 40, respectively. Finally, 96 and 50 FEs were adopted around the circumference and along the cylinder, respectively. Table 1 shows the convergence of the *in-vacuo* natural frequencies of the shell structure

Table 1
Convergence of FEM natural frequencies (*in-vacuo*) for cylindrical shell simply supported at its ends (Hz)

Mode (m,n)	1152 elements idealization	2048 elements idealization	3200 elements idealization	4800 elements idealization
1,5	96.1	96.0	96.0	96.0
2,5	242.0	241.2	240.9	240.7
3,5	398.6	396.5	395.6	395.1
4,5	524.2	521.4	520.2	519.6
5,5	618.1	616.1	615.2	615.0
1,6	104.8	104.7	104.6	104.6
2,6	205.3	204.8	204.5	204.4
3,6	341.4	339.4	338.6	338.1
4,6	467.4	464.0	462.5	461.8
5,6	572.0	568.1	566.6	565.8

for the first 10 mode shapes. The differences in the results, shown in Table 1, indicate that the calculated values are converging with increasing number of elements. The results of the final two idealizations (3200 and 4800 FEs models) may be considered as converged in terms of the natural frequencies.

Another test study was performed to obtain the converged hydrodynamic properties (generalized added mass, Coriolis force and centrifugal force coefficients) of the shell structure completely filled with flowing fluid. For this test study, various numbers of BEs (hydrodynamic panels) were distributed around the circumference and along the shell structure. The main aim of this study was to represent accurately the distortional *in-vacuo* mode shapes of the cylindrical shell. The hydrodynamic panels were distributed over the wetted surface of the structure as follows: one FE corresponding to one BE (hydrodynamic panel). Contrary to the previous study by Uğurlu and Ergin [14], a direct BE approach was employed in this study for the evaluation of potential function. Furthermore, a linear potential distribution over each hydrodynamic panel was considered instead of constant source distribution employed in Uğurlu and Ergin [14]. By using the linear distribution, the convergence of the hydrodynamic properties was achieved faster in terms of number of panels adopted in the calculations, compared with the constant distribution employed in Uğurlu and Ergin [14]. Fig. 2 presents the non-dimensional wet frequency values of the cylindrical shell containing flowing fluid as a function of the non-dimensional axial flow velocity for the first mode shape with $n = 5$ and for different hydrodynamic panel arrangements—four of which with constant potential distributions and one with the linear distribution, over the hydrodynamic panels. Furthermore, Fig. 2 presents the analytically calculated non-dimensional frequency values of Amabili and Garziera [5]. For the constant distributions, first, 64 and 32 hydrodynamic panels were, respectively, adopted around the circumference and along the shell for the shell completely filled with flowing fluid. In order to test the convergence with the constant potential distributions over the panels, the number of hydrodynamic panels around the circumference and along the structure, respectively, were first increased to 80 and 40, then to 96 and 50, and finally to 120 and 60. As seen from Fig. 2, the non-dimensional frequency values converge slowly with increasing number of hydrodynamic panels, and the frequency values with 120 and 60 panel distribution provides the best comparison with the analytical solution of Amabili and Garziera [5]. On the other hand, the BE method with linear distribution over the hydrodynamic panels provides the best comparison with the analytical solutions by using a very limited number of hydrodynamic panels over the wetted surface—48 panels around the circumference and 24 panels along the structure. This comparison shows the superiority of the higher-order distribution (linear distribution) over the constant one. The results presented in Fig. 2 correspond to the cylindrical shell with flexible extensions. This is to say that the cylindrical shell structure was assumed infinitely long and periodically supported, and a three-span length of the infinitely long flexible structure was adopted for the calculations. It was also assumed that the mode shapes are periodic functions with a main period of $2L$. Therefore, the mode shapes were anti-symmetric with respect to each support, and they were also the mode shapes with the lowest frequencies. For the results presented,

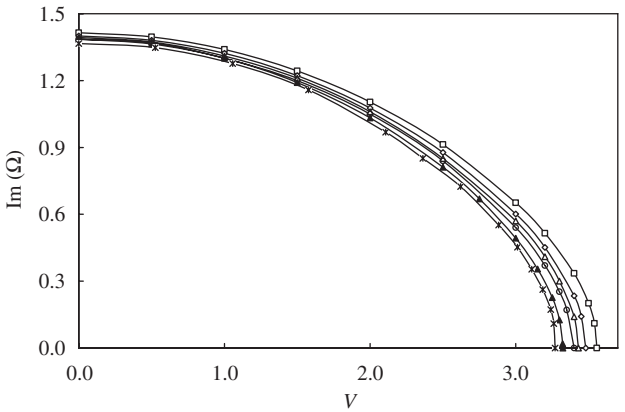

Fig. 2. Convergence of non-dimensional frequencies of fluid conveying simply supported cylindrical shell with flexible extensions for first axial mode, with $n = 5$. Key: (—□—) 64–32 (C); (—◇—) 80–40 (C); (—△—) 96–50 (C); (—○—) 120–60 (C); (—▲—) 48–24 (L); and (—✳—) Amabili and Garziera [5] (C and L indicate constant and linear distributions, respectively).

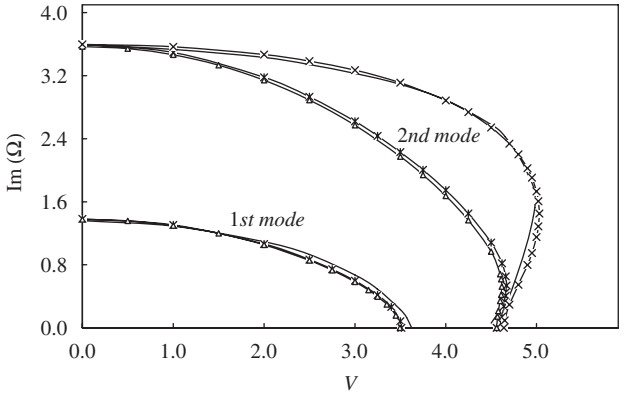

Fig. 3. Imaginary parts of non-dimensional eigenvalues of fluid conveying simply supported cylindrical shell with rigid extensions for first two axial modes with $n = 5$. Key: ( ) 48–24; ( ) 64–32; ( ) 48–24 (two modes); and ( ) Weaver and Unny [28].

a maximum number of 12 *in-vacuo* modes were included in the analysis—6 of which were symmetric and 6 anti-symmetric with respect to the symmetry plane through the center of the shell along the structure.

In Fig. 3, the calculated non-dimensional frequency values are presented as a function of non-dimensional flow velocity for the first and second axial mode shapes with the circumferential wavenumber, $n = 5$, and for two different panel distributions with the linear potential variation over the panels. In the first idealization, 48 panels around the circumference and 24 panels along the shell structure were adopted, and in a further test study, the number of hydrodynamic panels around the circumference and along the structure was increased to 64 and 32, respectively. The predictions of this study were compared with the results of Weaver and Unny [28]. It can be seen from the figure that the calculations with 48–24 and 64–32-panel idealizations give similar results. Furthermore, the predictions for the first axial mode compare very well with Weaver and Unny [28], but the results for the second axial mode do not compare well with the results of Weaver and Unny [28]. The calculations were repeated adopting only the first two axial *in-vacuo* modes with $n = 5$ and using the panel idealization 48–24, and these predictions compare with the results of Weaver and Unny [28] very well. The calculations by Weaver and Unny [28] employed only two axial modes with the circumferential wavenumber, $n = 5$. It can be said that the results of Weaver and Unny [28], especially, for the second mode are not sufficiently converged. On the other hand, the results of this study presented in Fig. 3 correspond to the cylindrical shell with rigid extensions. This is to say that the flexible cylindrical shell is connected to infinitely long rigid cylindrical baffles, of the same diameter as the shell, at both ends. The kinematic boundary conditions (Eqs. (13a) and (13b)) was imposed on the flexible shell, and the rigid boundary wetted surface condition $\partial\phi/\partial n = 0$ was employed for the rigid extensions.

Fig. 4 compares the imaginary parts of the predicted non-dimensional eigenvalues (*wet* frequencies) with those obtained by Selmane and Lakis [29], Amabili et al. [9] and Amabili and Garziera [5], for the first two *wet* modes having five circumferential waves ($n = 5$). In these calculations, the shell structure was assumed with flexible extensions at both ends, and a linear potential distribution was assumed over each panel. As seen from the results presented, the idealizations with 48–24, and 64–32 panels around the circumference and along the shell, respectively, give almost the same results, and compare well with the analytical results found in literature. Furthermore, in Figs. 5(a) and (b), the real and imaginary parts of the non-dimensional eigenvalues are presented for the first three axial mode shapes with the circumferential wavenumber, $n = 5$. For the results presented in these figures, the cylindrical shell is considered with rigid extensions. As seen in Fig. 5(b), the imaginary part of the non-dimensional eigenfrequency decreases with increasing non-dimensional axial flow velocity. The first mode shape reaches its zero frequency at $V = 3.495$, and re-stabilizes again at the axial flow velocity, $V = 4.56$. Then the first and second modes merge at $V = 4.62$ and this point corresponds to the onset of the coupled-mode flutter. It should be noted that the coupled-mode flutter cannot be decided by the linear theory. Furthermore, the real part of the non-dimensional eigenfrequency is presented in Fig. 5(a) as a function of the non-dimensional flow velocity, and it is proportional to damping. It should also be noted that

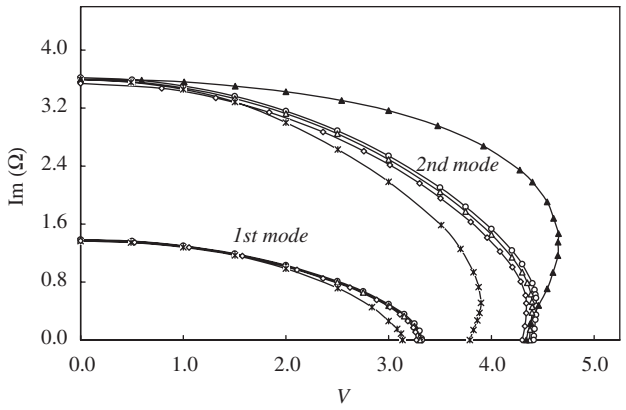

Fig. 4. Imaginary parts of non-dimensional eigenvalues of fluid conveying simply supported cylindrical shell with flexible extensions for first two axial modes with $n = 5$. Key: (—○—) 48–24; (—△—) 64–32; (—✳—) Selmane and Lakis [29]; (—▲—) Amabili et al. [9]; and (—◇—) Amabili and Garziera [5].

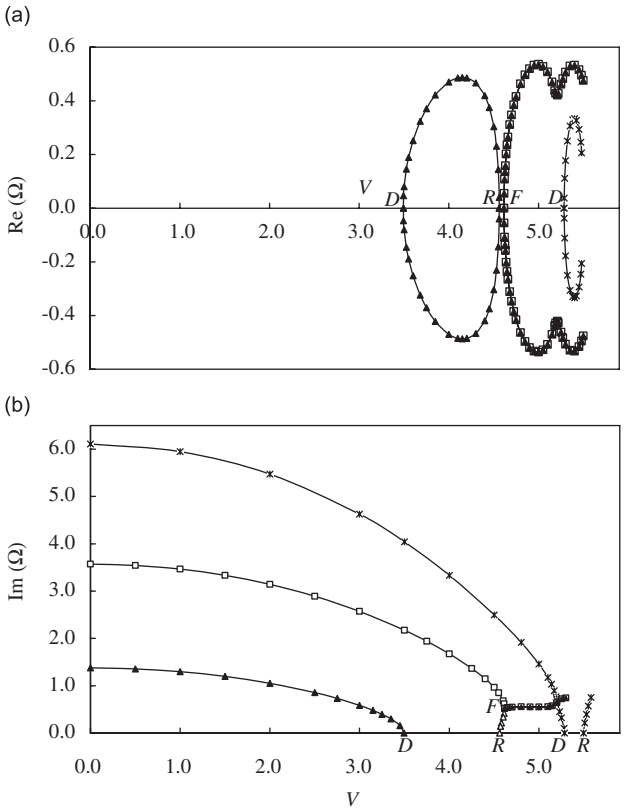

Fig. 5. Non-dimensional eigenvalues of fluid conveying simply supported cylindrical shell with rigid extensions, for $n = 5$: (a) real parts and (b) imaginary parts. Key: (—▲—) first mode, (—□—) second mode, and (—✳—) third mode.

the system is stable when the real part of the non-dimensional frequency (Ω) is negative, and it is unstable when the real part of Ω is positive.

In order to demonstrate the difference between the models with rigid and flexible extensions, the non-dimensional wet frequencies are presented together in Fig. 6 for the models with rigid and flexible extensions, for the first two wet axial modes and the circumferential wavenumber, $n = 5$. It can be observed from Fig. 6

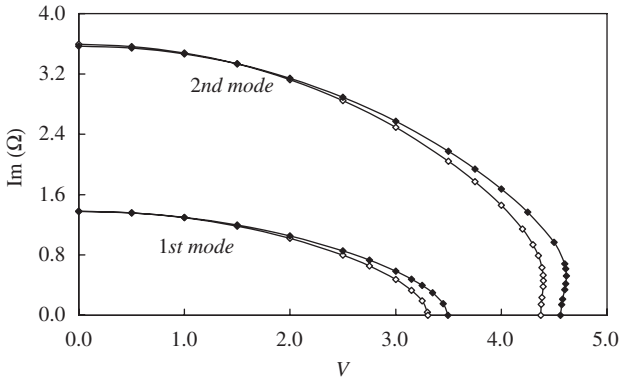

Fig. 6. Imaginary parts of non-dimensional eigenvalues for first two axial modes, with $n = 5$, of fluid conveying simply supported cylindrical shell. Key: (—◇—) with elastic extensions and (—◆—) with rigid extensions.

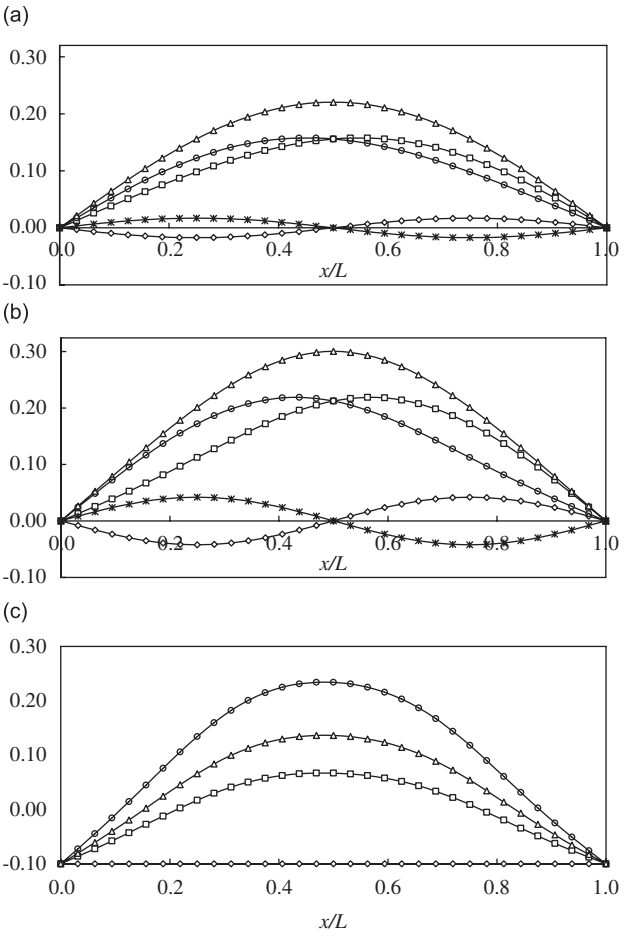

Fig. 7. First eigenmode of fluid conveying simply supported cylindrical shell, for $n = 5$: (a) $V = 1.05$, (b) $V = 3.15$, and (c) $V = 3.49$. Key: (—◇—) $t = 0$, (—□—) $t = T/8$, (—△—) $t = T/4$, (—○—) $t = 3T/8$, and (—✳—) $t = T/2$ (T is period).

that the model with flexible extensions predicts slightly lower wet frequency values in comparison with the model with rigid extensions. This is due to an increase in the generalized fluid stiffness forces.

Figs. 7(a)–(c) present the first wet mode shape, with $n = 5$, of the cylindrical shell completely filled with flowing fluid at the times $t = 0$, $T/8$, $T/4$, $3T/8$ and $T/2$ (where T is the time period) for the non-dimensional

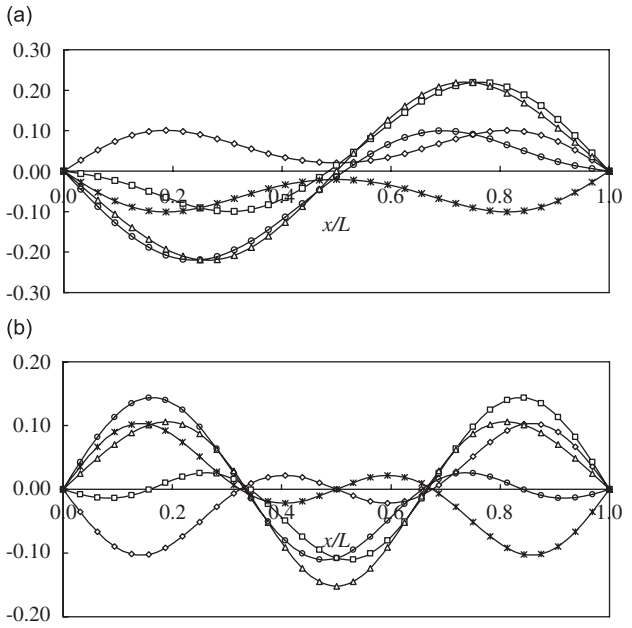

Fig. 8. Eigenmodes of fluid conveying simply supported cylindrical shell, for $n = 5$ and $V = 1.75$: (a) second mode and (b) third mode. Key: (—◇—) $t = 0$, (—□—) $t = T/8$, (—△—) $t = T/4$, (—○—) $t = 3T/8$ and (—✳—) $t = T/2$.

flow velocities $V = 1.05$, 3.15 and 3.49 (corresponding, respectively, to $0.3V_d$, $0.9V_d$ and V_d), respectively. V_d represents the non-dimensional flow velocity at the divergence. It should be noted that the mode shapes are complex due to the effect of Coriolis fluid–structure interaction forces. The real part of the first eigenvector has one longitudinal half-wave and the imaginary part has two longitudinal half-waves (see mode shapes at $t = 0$ and $T/2$ in Figs. 7(a) and (b)). Furthermore, in Figs. 8(a) and (b), the second and third axial eigenmodes are presented at the times $t = 0$, $T/8$, $T/4$, $3T/8$ and $T/2$ for the non-dimensional flow velocity, $V = 1.745$ ($0.5V_d$). As can be observed from these figures, the mode shapes involves mainly the first three axial half-waves.

3.2. Cylindrical shell clamped at both ends

Another series of calculations were performed to investigate the dynamic response of a cylindrical shell structure clamped at both ends. The shell structure adopted is a long cylindrical shell, and it was previously studied by Païdoussis et al. [30] and Misra et al. [31], analytically. The shell has the following geometrical and material properties: length $L = 1\,\text{m}$, radius $R = 90\,\text{mm}$, thickness $h = 0.5\,\text{mm}$, Young's modulus $E = 106\,\text{GPa}$, Poisson's ratio $\nu = 0.3$, and mass densities $\rho_s = 7715\,\text{kg/m}^3$ and $\rho_f = 998.6\,\text{kg/m}^3$.

In Fig. 9, the non-dimensional wet frequency values are presented as a function of the non-dimensional axial flow velocity for the first two axial mode shapes with the circumferential wavenumber, $n = 3$, and they are compared with the results of Misra et al. [31]. For the first two axial modes with $n = 3$, the non-dimensional critical flow velocities are calculated as 17.84 and 21.82, respectively, and they compare well with the results of 17.83 and 21.62, respectively, predicted by Misra et al. [31]. However, in the vicinity of the coupled-mode flutter, the differences between the predictions of this study and those of Misra et al. [31] increase, and a maximum of 6.7% difference is observed between the results. Misra et al. [31] performed the calculations by using the Galerkin method and employing the first three axial waves with the circumferential wavenumber, $n = 3$. However, in the present study, the first six axial waves with $n = 3$ were adopted for the calculations. Therefore, it may be said that these differences would be mainly due to the limited number of axial modes adopted in the study of Misra et al. [31].

In a further study, the shell structure adopted in Section 3.1 was studied with clamped ends. The non-dimensional wet frequency values are presented in Figs. 10(a) and (b) for the first and second axial modes,

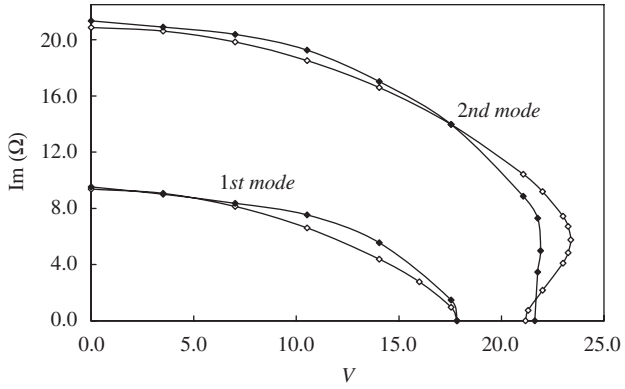

Fig. 9. Imaginary parts of non-dimensional eigenvalues for first two axial modes, with $n = 3$, of fluid conveying cylindrical shell clamped at both ends. Key: (—◇—) this study and (—◆—) Misra et al. [31].

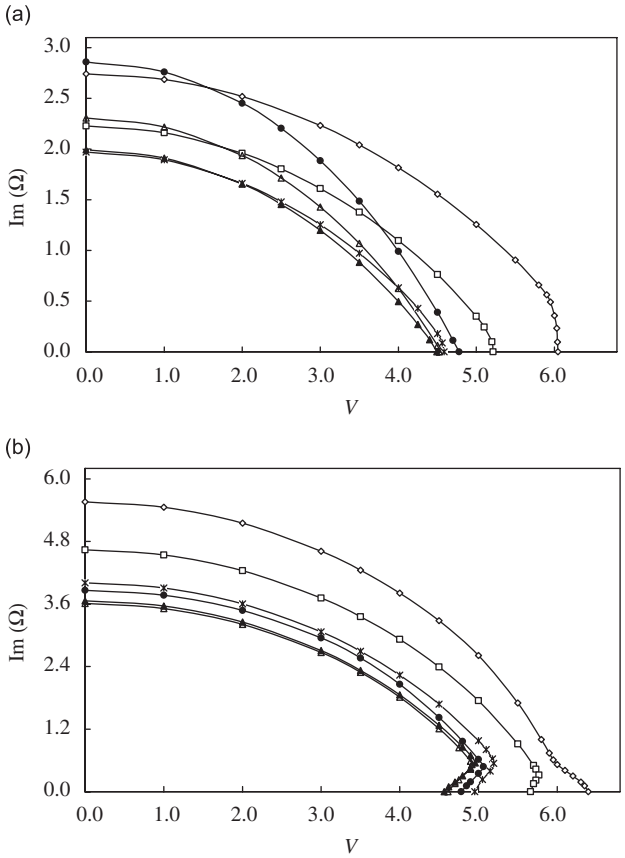

Fig. 10. Imaginary parts of non-dimensional eigenvalues for fluid conveying cylindrical shell clamped at both ends, with rigid extensions: (a) first mode and (b) second mode. Key: (—◇—) $n = 3$, (—□—) $n = 4$, (—✳—) $n = 5$, (—▲—) $n = 6$, (—△—) $n = 7$, and (—●—) $n = 8$.

respectively, and for the circumferential wavenumbers, $n = 3$–8. The non-dimensional wet frequency values decrease with increasing non-dimensional axial flow velocity, and the divergence is observed for the mode shape with the circumferential wavenumber, $n = 6$ (see Fig. 10(a)). As the flow velocity increases, for the circumferential wavenumbers, $n = 4$–8, the shell structure first gains its stability, and then the coupled-mode

flutter follows. For the results presented in Figs. 10(a) and (b), the cylindrical shell was assumed with rigid extensions at both ends.

On the other hand, the shell structure completely filled with the flowing fluid exhibits the Païdoussis-type vibrations for the circumferential wavenumber, $n = 3$. For this circumferential wavenumber, the first two critical velocities correspond to a divergence. It is to say that the coupled-mode flutter originates directly from a divergent state, without stabilization between these instability states. This is known in the literature as *Païdoussis coupled-mode flutter* (see, for instance, Ref. [32]).

By comparing Figs. 10(a)–(b) with Fig. 6, it can be realized that the non-dimensional wet frequencies of the clamped ended shell are always higher than those of the flexible cylindrical shell with simply supported ends. This is expected due to that the clamped ends increase the stiffness of the cylindrical structure in comparison with the cylindrical shell with simply supported ends. On the other hand, it is also observed that the shell with clamped ends will have divergences at higher axial flow velocities compared with the simply supported shell.

Furthermore, the calculations were repeated for the cylindrical shell with clamped ends and with flexible extensions at both ends. For the calculations of the fluid–structure interaction forces, a three-span length of the shell structure was adopted and the interaction effects were calculated for the middle span of the three-span system. These results are presented in Fig. 11 for the first axial mode shape and the circumferential wavenumbers, $n = 3$–8. From the comparison of Figs. 10 and 11, it can be observed that the critical flow velocities become slightly lower for the shell with flexible extensions, compared with those for the shell with rigid extensions.

3.3. Asymmetric support conditions (pinned–clamped)

In this part of the study, the cylindrical shell was considered as simply supported at the upstream end and clamped at the downstream one (pinned–clamped). The circular cylindrical shell structure investigated in Section 3.1 is again adopted for the calculations. This problem (a cylindrical shell with pinned–clamped ends) was first time studied by Horáček and Zolotarev [33], and they wrongly claimed that the clamped–pinned and pinned–clamped shells were non-conservative for all values of the axial flow velocity. Later, it was shown by Misra et al. [31] and Amabili and Garizera [5] that the pinned–clamped or clamped–pinned cylindrical shells conveying fluid flow behave as conservative systems.

For the cylindrical shell with simply supported and clamped ends, respectively, at the upstream and downstream ends, the real part of the non-dimensional eigenvalues (damping coefficient) is presented as a function of the non-dimensional axial flow velocity in Fig. 12 for the first two axial mode shapes with the circumferential wavenumber, $n = 5$. After the structure regains its stability at the non-dimensional flow velocity, $V = 3.96$, for a short range of the non-dimensional axial flow velocity ($4.84 < V < 4.91$), the damping coefficient becomes zero as observed from Fig. 12. It may also be further said, as in Païdoussis [4], that the clamped–pinned and pinned–clamped cylindrical shells conveying flowing fluid are conservative systems as clamped–clamped and pinned–pinned (simply supported at both ends) ones are.

By reversing the axial flow direction, the shell becomes clamped at the upstream end and simply supported at the down stream end. It is known that the centrifugal fluid–structure interaction force coefficient is proportional to the square of the flow velocity, and therefore its sign and magnitude are not affected from this change in flow direction. However, the matrix of Coriolis force coefficients is anti-symmetric for conservative systems, and hence a change in the axial flow direction results in a sign change in the off-diagonal terms of this matrix. Therefore, the response behavior the shell structure clamped at the upstream and simply supported at the down stream ends remains same with that of the cylindrical shell simply supported at the upstream and clamped at the down stream end.

Figs. 13(a) and (b) present the non-dimensional wet eigenfrequencies of the cylindrical shell as a function of the non-dimensional axial flow velocity for the first two axial mode shapes with the circumferential wavenumbers, $n = 4$–8. It may seen from these figures that, for the shell structure, the divergence occurs for the circumferential wavenumber, $n = 5$. The wet frequencies behave as expected. It is to say that the frequency values decrease with increasing axial flow velocity, and that they reach zero values at certain non-dimensional axial flow velocities (see Figs. 13(a) and (b)). The cylindrical shell regains its stability at the non-dimensional critical flow velocities seen in Fig. 13(b) for each associated circumferential wavenumber. By comparing

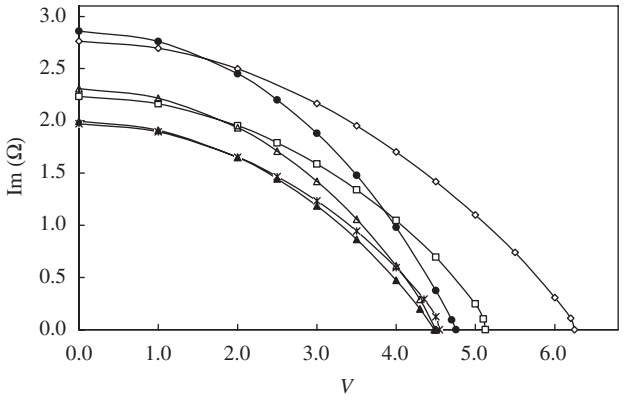

Fig. 11. Imaginary parts of non-dimensional eigenvalues for first mode of fluid conveying cylindrical shell clamped at both ends, with flexible extensions: Key: (—◇—) $n = 3$, (—□—) $n = 4$, (—✳—) $n = 5$, (—▲—) $n = 6$, (—△—) $n = 7$, and (—●—) $n = 8$.

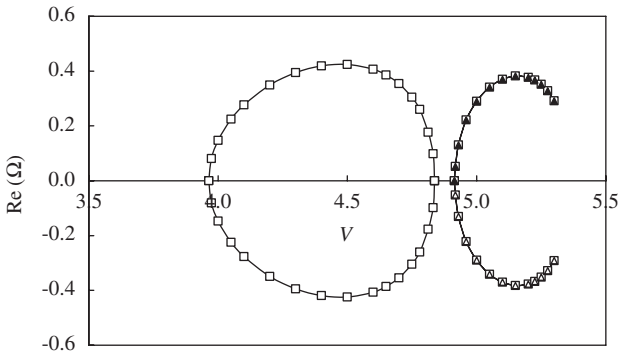

Fig. 12. Real parts of non-dimensional eigenvalues for first two axial modes, with $n = 5$, of fluid conveying cylindrical shell with pinned-clamped ends: Key: (—□—) first mode and (—▲—) second mode.

Figs. 6, 10(a)–(b) and 13(a)–(b), it can be seen that the non-dimensional frequency values for the clamped–pinned cylindrical shell lies between those for the shell structures with simply supported ends and clamped ends.

3.4. Cantilever cylindrical shell conveying flowing fluid

In order to test the method of analysis for the unconservative fluid–structure interaction systems, a group of cantilever cylindrical shells conveying flowing fluid was adopted for the calculations. The circular cylindrical shell structures used for the calculations has the following geometrical and material properties: thickness-to-radius ratio $h/R = 0.0227$, fluid–shell density ratio $\mu = (R\rho_f)/(h\rho_s) = 0.06$ and Poisson's ratio $\nu = 0.5$. The critical flow velocities at which a flutter initiated were calculated, and they are presented in Fig. 14 as a function of the length-to-radius ratio and compared with the results of Païdoussis and Dennis [34], and Shayo and Ellen [35]. Because the density of the flowing fluid is lower compared with the fluids used in Sections 3.1 and 3.2, the instabilities occur at relatively higher flow velocities, and therefore, the following formulation was used in stead of Eq. (26) for non-dimensionalizing axial flow velocities presented in Fig. 14: $V = U/(E/\rho_s(1-\nu^2))^{1/2}$ as in Païdoussis and Dennis [34]. For the investigated cantilever shells in contact with flowing fluid, the flutter is generally observed at the second axial modes or rarely at the third axial modes, contrary to the conservative flowing fluid–shell systems having a divergence at the first axial mode.

As seen from Fig. 14, for the lower length-to-radius ratios ($L/R < 10$), the critical flow velocity decreases with increasing circumferential wavenumber. For the higher length-to-radius ratios ($L/R > 10$), the critical

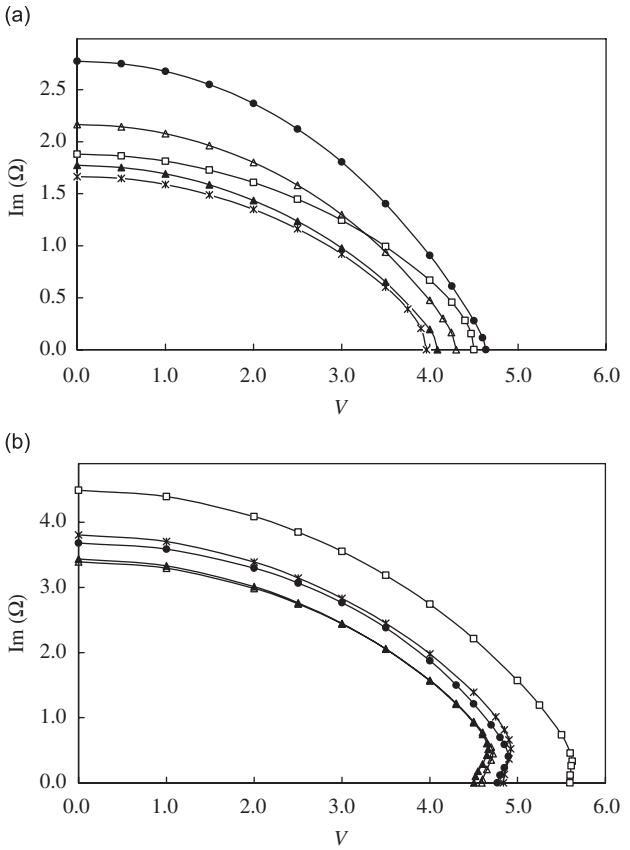

Fig. 13. Imaginary parts of non-dimensional eigenvalues for fluid conveying cylindrical shell with pinned–clamped ends: (a) first mode and (b) second mode. Key: (—□—) $n=4$, (—✳—) $n=5$, (—▲—) $n=6$, (—△—) $n=7$, and (—●—) $n=8$.

flow velocities for the modes with $n=2$ become higher than those with $n=3$. For all the L/R ratios investigated, the highest critical flow velocities are observed for the circumferential wavenumber, $n=1$. It should also be mentioned that the flow velocities above the critical velocity curves indicate a dynamically unstable behavior for the shell-flowing fluid system.

Another group of calculations was performed for a cantilever cylindrical shell structure with the following material and geometrical properties: length-to-radius ratio $L/R=5$, thickness-to-radius ratio $h/R=0.01$, Young's modulus $E=206\,\text{GPa}$, Poisson's ratio $v=0.3$, structural density $\rho_s=7850\,\text{kg/m}^3$ and fluid density $\rho_f=1000\,\text{kg/m}^3$. The calculated non-dimensional complex eigenvalues are presented in Fig. 15 as a function of the non-dimensional flow velocity for the first three axial wet modes with the circumferential wavenumber, $n=2$. For non-dimensionalizing axial flow velocity, Eq. (26) is again adopted here. It is seen from Fig. 15 that the system undergoes damped oscillations in all the modes. It may also be said that the flow results in changes in the natural frequencies and contributes to damping. It is also observed from Fig. 15 that, on the contrary to the conservative fluid–structure systems, the cantilever cylindrical shell with the axial flow exhibits different response characteristics for the each wet eigenmode. Due to the effect of the centrifugal fluid–structure interaction forces, for the first wet mode, the non-dimensional eigenfrequency decreases with increasing non-dimensional axial flow velocity, and the system loses its rigidity at the non-dimensional axial flow velocity, $V=8.51$. However, the system is still not in a state of divergence. The shell-flow system gains its stability again at $V=15.15$, and then the wet frequency increases with increasing flow velocity. On the other hand, the non-dimensional damping coefficient decreases with increasing flow velocity until the non-dimensional flow velocity reaches the value of 15.15, and then it changes its tendency and increases with increasing flow velocity, as seen in Fig. 15. After the non-dimensional flow velocity, $V=18.25$, the non-dimensional wet frequency for the first wet mode with $n=2$ decreases with increasing flow velocity and loses its rigidity at $V=19.45$ and the

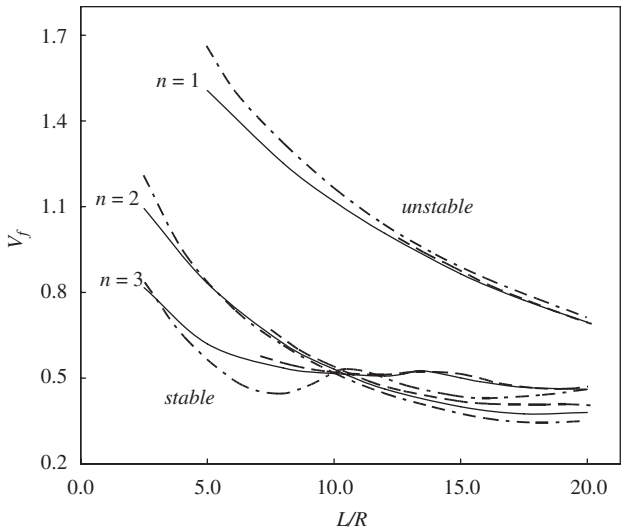

Fig. 14. Critical non-dimensional flow velocities of fluid conveying cantilever cylindrical shells as a function of L/R, for $n = 1$–3. Key: (_____) this study, (__.__.__.__) Shayo and Ellen [35], and (_ _ _ _ _ _ _) Paidoussis and Dennis [34].

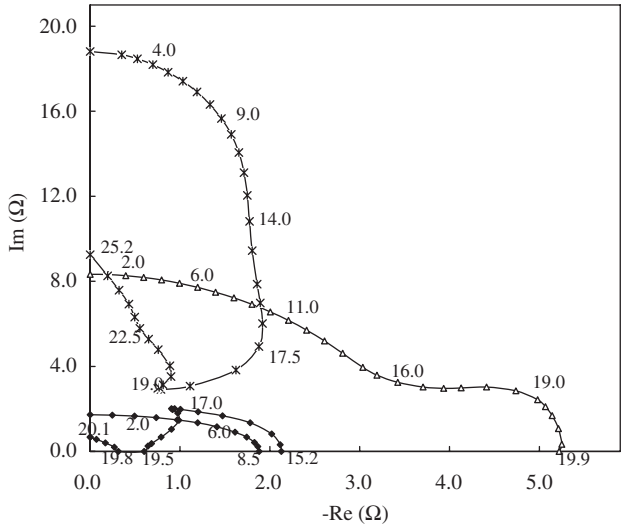

Fig. 15. Non-dimensional complex eigenvalues of first three modes, with $n = 2$ for fluid conveying cantilever cylindrical shell: Key: (—◆—) first mode, (—△—) second mode and (—✳—) third mode.

shell–fluid system, once more, gains its stability at $V = 19.76$. At the non-dimensional flow velocity $V = 20.08$, the damping coefficient changes its sign from negative to positive, and it is to say that this flow velocity corresponds to the onset of flutter for the first wet eigenmode with the circumferential wavenumber, $n = 2$. The dynamic response behavior of the second and third wet eigenmodes with $n = 2$ can also be observed from Fig. 15. It may be concluded from the figure that a divergence is present for the second mode at the non-dimensional axial flow velocity, $V = 19.9$ and a flutter for the third mode at $V = 25.2$.

The first three wet eigenmodes with $n = 2$ are presented in Figs. 16(a)–(c) at times $t = 0$, $T/8$, $T/4$, $3T/8$, $T/2$, $5T/8$, $3T/4$ and $7T/8$ (where T is the time period), respectively, for the non-dimensional axial flow velocities, $V = 17$, 21.59 and 19. As seen from Figs. 16(a) and (c), the first and third mode shapes are mainly dominated by the dry eigenmodes with the axial half-waves, $m = 1$ and 2. However, all the dry modes included in the calculations contribute to the wet modes shapes in some degree. It should also be noted that the mode shapes are complex. In the conservative systems, the phase angle takes on the values of zero, $\pi/2$ or their multiples.

However, in the non-conservative systems such as the cantilever shell containing an axial flow, the phase angle can take on any numerical value.

The second wet eigenmode in Fig. 16(b) is presented for the non-dimensional axial flow velocity, $V = 21.59$, and this velocity corresponds to an axial flow velocity just before the occurrence of divergence. The dry eigenmodes contribute to the second mode at equal phase angles, and therefore the mode shape in a period of T is preserved, as seen in Fig. 16(b).

3.5. A tapered circular cylindrical shell conveying flowing fluid

Another group of calculations was performed for a tapered circular cylindrical shell conveying flowing fluid and simply supported at both ends with rigid extensions. The tapered cylindrical shell was chosen in order to apply the method of analysis to a structure not studied before. The calculations were carried out for three different radius ratios $R_d/R_u = 0.90$, 0.95 and 1. R_u and R_d represent, respectively, the radius of the cylindrical shell at the up stream and down stream ends as seen in Fig. 17(a). The tapered cylindrical shell adopted for the calculations has the following geometrical and material properties: length-to-radius ratio

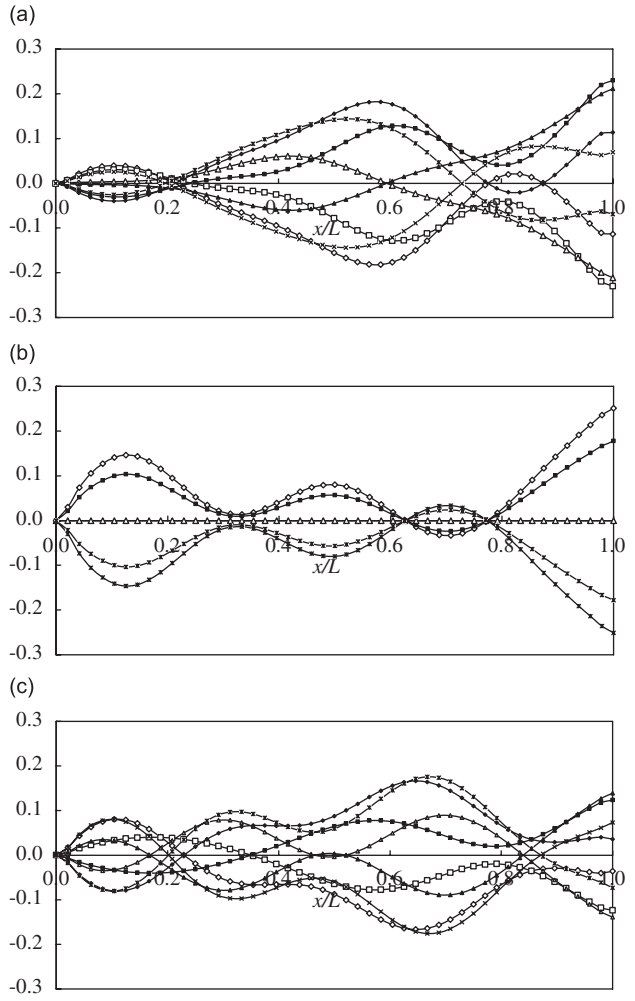

Fig. 16. Eigenmodes of fluid conveying cantilever cylindrical shell, for $n = 2$: (a) first mode for $V = 17.00$, (b) second mode for $V = 21.59$, and (c) third mode for $V = 19$. Key: (—◇—) $t = 0$, (—□—) $t = T/8$, (—△—) $t = T/4$, (—✳—) $t = 3T/8$, (—◆—) $t = T/2$, (—■—) $t = 5T/8$, (—▲—) $t = 3T/4$ and (—✕—) $t = 7T/8$.

$L/R_u = 2$, thickness-to-radius ratio $h/R_u = 0.01$, Young's modulus $E = 206\,\text{GPa}$, Poisson's ratio $\nu = 0.3$, and mass density $\rho_s = 7850\,\text{kg/m}^3$. Fresh water is used as the contained fluid with a density of $\rho_f = 1000\,\text{kg/m}^3$.

The converged *in-vacuo* dynamic properties and corresponding hydrodynamic characteristic values (generalized added mass, generalized hydrodynamic force coefficients and generalized fluid stiffness coefficients) were obtained by using 64 and 32 FEs/BEs, respectively, around and along the shell structure. For the results presented in Fig. 17(b), a number of 12 *in-vacuo* modes were included in the analysis—six of which were symmetric and six anti-symmetric with respect to the symmetry plane through the center of the shell along the structure.

In Fig. 17(b), the calculated non-dimensional frequency values are presented as a function of non-dimensional flow velocity for the first and second axial mode shapes with the circumferential wavenumber, $n = 5$. The results are presented for the ratios $R_d/R_u = 0.90$, 0.95 and 1. As observed from Fig. 17(b), the non-dimensional frequency values increase with increasing ratio R_d/R_u. The first axial mode shape reaches its zero frequency at $V = 3.23$, 3.33 and 3.49 for the ratios of $R_d/R_u = 0.90$, 0.95 and 1, respectively. The mode shape re-stabilizes again at the non-dimensional axial flow velocities $V = 4.08$, 4.31 and 4.56, respectively, for $R_d/R_u = 0.90$, 0.95 and 1. Then the first and second modes merge at $V = 4.16$, 4.37 and 4.61 for the ratios of $R_d/R_u = 0.90$, 0.95 and 1, respectively, and these points correspond to the onset of the coupled-mode flutter (not shown in Fig. 17(b)).

4. Conclusions

The dynamic response behaviors (non-dimensional eigenvalues and modes) of the cylindrical shell structures containing flowing fluid with various end conditions, such as simply supported, clamped–clamped, clamped–pinned and clamped–free (cantilever shell) ends, were calculated by using a hybrid method—a boundary integral method for calculating the fluid–structure interaction effects and a FE method for obtaining the *in-vacuo* dynamic properties of the structure. In a further analysis, a tapered cylindrical shell conveying flowing fluid and simply supported at its ends was investigated. The method used in this study was already successfully applied to a circular cylindrical shell containing and/or submerged in flowing fluid, with

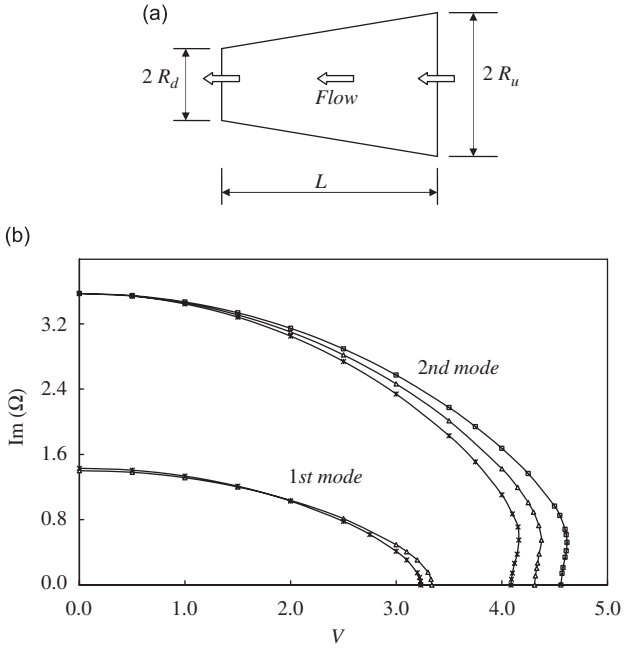

Fig. 17. (a) Tappered cylindrical shell simply supported at its ends and containing flowing fluid and (b) non-dimensional eigenvalues for tapered cylindrical shell. Key: (—□—) $R_d/R_u = 1.0$, (—△—) $R_d/R_u = 0.95$, and (—×—) $R_d/R_u = 0.90$.

simply supported ends (see Ref. [14]). It can be said that the hybrid method introduced in this study can be applied to any shape of cylindrical structure partially in contact with internal and/or external flowing fluid, in contrast to the studies found in the literature.

For the convergence of the *in-vacuo* dynamic properties, various numbers of FEs were distributed over the wetted surface of the shell structures. Furthermore, another convergence study was also performed for the hydrodynamic properties (generalized added mass, generalized Coriolis fluid force coefficient, generalized centrifugal fluid force coefficient) of the shell structures. In order to test the convergence of the hydrodynamic fluid–structure interaction effects, various numbers of BEs (so-called hydrodynamic panels) were distributed over the wetted surface of the cylindrical shells (one FE corresponding to one hydrodynamic panel).

The predicted non-dimensional frequency values were compared with the analytical solutions found in the literature, and a very good comparison was obtained. It should be said that the predicted frequency values behave as expected. It is to say that they decrease with increasing non-dimensional axial flow velocity, and they reach a zero frequency for the axial flow velocity at which a divergence occurs, for conservative fluid–structure interaction systems. On the other hand, for the non-conservative fluid–structure problem (cantilever cylindrical shell containing axial flow), the fluid damping is always present in the system.

The circular cylindrical shells-containing flowing fluid behaves conservatively with the simply supported ends, clamped–clamped ends, and with the clamped–simply supported ends. However, the cantilever circular cylindrical shell possesses a non-conservative dynamic system when subjected to an axial flow. These dynamic response behaviors were demonstrated through the numerical calculations.

The present study has demonstrated the versatility of the method, developed before and extended in this study further. By introducing the linearly varying BEs, the convergence of the numerical predictions were obtained much faster than those using constant distributions over the BEs in the previous study [14]. In a future study, the effect of free surface waves on the dynamic response behavior will be considered.

Acknowledgment

This research was financially supported by the Scientific and Technological Research Council of Turkey (TUBITAK Project no. 105M041). This support is gratefully acknowledged.

References

[1] M.P. Païdoussis, Flow-induced instabilities of cylindrical structures, *Applied Mechanics Reviews* 40 (1987) 163–175.
[2] M.P. Païdoussis, G.X. Li, Pipes conveying fluid: a model dynamic problem, *Journal of Fluids and Structures* 7 (1993) 137–204.
[3] M.P. Païdoussis, *Fluid–structure Interactions: Slender Structures and Axial Flow*, Vol. I, Academic Press, London, 1998.
[4] M.P. Païdoussis, *Fluid–structure Interactions: Slender Structures and Axial Flow*, Vol. II, Elsevier, The Netherlands, 2004.
[5] M. Amabili, R. Garziera, Vibrations of circular cylindrical shells with nonuniform constraints, elastic bed and added mass. Part II: shells containing or immersed in axial flow, *Journal of Fluids and Structures* 16 (2002) 31–51.
[6] M.P. Païdoussis, E. Grinevich, D. Adamovic, C. Semler, Linear and nonlinear dynamics of cantilevered cylinders in axial flow, Part 1: physical dynamics, *Journal of Fluids and Structures* 16 (2002) 691–713.
[7] J.L. Lopes, M.P. Païdoussis, C. Semler, Linear and nonlinear dynamics of cantilevered cylinders in axial flow, Part 2: the equations of motion, *Journal of Fluids and Structures* 16 (2002) 715–737.
[8] C. Semler, J.L. Lopes, N. Augu, M.P. Païdoussis, Linear and nonlinear dynamics of cantilevered cylinders in axial flow, Part 3: nonlinear dynamics, *Journal of Fluids and Structures* 16 (2002) 739–759.
[9] M. Amabili, F. Pellicano, M.P. Païdoussis, Non-linear dynamics and stability of circular cylindrical shells containing flowing fluid, Part 1: stability, *Journal of Sound and Vibration* 225 (1999) 655–699.
[10] M. Amabili, F. Pellicano, M.P. Païdoussis, Nonlinear stability of circular cylindrical shells in annular and unbounded axial flow, *Journal of Applied Mechanics-American Society of Mechanical Engineers* 68 (2001) 827–834.
[11] M. Amabili, F. Pellicano, M.P. Païdoussis, Non-linear dynamics and stability of circular cylindrical shells conveying flowing fluid, *Computers and Structures* 80 (2002) 899–906.
[12] M.A. Langthjem, N. Olhoff, Modal expansion of the perturbation velocity potential for a cantilevered fluid-conveying cylindrical shell, *Journal of Fluids and Structures* 17 (2003) 147–161.
[13] K.N. Karagiozis, M.P. Païdoussis, A.K. Misra, E. Grinevich, An experimental study of the nonlinear dynamics of cylindrical shells with clamped ends subjected to axial flow, *Journal of Fluids and Structures* 20 (2005) 801–816.
[14] B. Uğurlu, A. Ergin, A hydroelasticity method for vibrating structures containing and/or submerged in flowing fluid, *Journal of Sound and Vibration* 290 (2006) 572–596.

[15] A.A. Lakis, A. Selmane, Hybrid finite element analysis of large amplitude vibration of orthotropic open and closed cylindrical shells subjected to a flowing fluid, *Nuclear Engineering and Design* 196 (2000) 1–15.
[16] M.H. Toorani, A.A. Lakis, Shear deformations in dynamic analysis of anisotropic laminated open cylindrical shells filled with or subjected to a flowing fluid, *Computer Methods in Applied Mechanics and Engineering* 190 (2001) 4929–4966.
[17] M.H. Toorani, A.A. Lakis, Dynamic analysis of anisotropic cylindrical shells containing flowing fluid, *Journal of Pressure Vessel Technology-American Society of Mechanical Engineers* 123 (2001) 454–460.
[18] M.H. Toorani, A.A. Lakis, Dynamic behavior of axisymmetric and beam-like anisotropic cylindrical shells conveying fluid, *Journal of Sound and Vibration* 259 (2003) 265–298.
[19] Y.L. Zhang, J.M. Reese, D.G. Gorman, Finite element analysis of the vibratory characteristics of cylindrical shells conveying fluid, *Computer Methods in Applied Mechanics and Engineering* 191 (2002) 5207–5231.
[20] Y.L. Zhang, J.M. Reese, D.G. Gorman, A comparative study of axisymmetric finite elements for the vibration of thin cylindrical shells conveying fluid, *International Journal for Numerical Methods in Engineering* 54 (2002) 89–110.
[21] M. Amabili, R. Garziera, Vibrations of circular cylindrical shells with nonuniform constraints, elastic bed and added mass; Part III: steady viscous effects on shells conveying fluid, *Journal of Fluids and Structures* 16 (2002) 795–809.
[22] ANSYS, *User's Manual*, ANSYS Inc., Houston, 1994.
[23] A. Ergin, W.G. Price, R. Randall, P. Temarel, Dynamic characteristics of a submerged, flexible cylinder vibrating in finite water depths, *Journal of Ship Research* 36 (1992) 154–167.
[24] A. Ergin, B. Uğurlu, Linear vibration analysis of cantilever plates partially submerged in fluid, *Journal of Fluids and Structures* 17 (2003) 927–939.
[25] A. Ergin, P. Temarel, Free vibration of a partially liquid-filled and submerged, horizontal cylindrical shell, *Journal of Sound and Vibration* 254 (2002) 951–965.
[26] L.C. Wrobel, *The Boundary Element Method, Applications in Thermo-fluid and Acoustics*, Vol. 1, Wiley, New York, 2002.
[27] B. Uğurlu, Hydro-elastic Analysis of High Frequency Elastic Structures Partially in Contact with Internal and External Fluids, Ph.D. Thesis, Istanbul Technical University, Istanbul, Turkey, 2006 (in Turkish).
[28] D.S. Weaver, T.E. Unny, On the dynamic stability of fluid-conveying pipes, *Journal of Applied Mechanics-American Society of Mechanical Engineers* 40 (1973) 48–52.
[29] A. Selmane, A.A. Lakis, Vibration analysis of anisotropic open cylindrical shells subjected to a flowing fluid, *Journal of Fluids and Structures* 11 (1997) 111–134.
[30] M.P. Païdoussis, S.P. Chan, A.K. Misra, Dynamics and stability of coaxial cylindrical shells containing flowing fluid, *Journal of Sound and Vibration* 97 (1984) 201–235.
[31] A.K. Misra, S.S.T. Wong, M.P. Païdoussis, Dynamics and stability of pinned–clamped and clamped–pinned cylindrical shells conveying fluid, *Journal of Fluids and Structures* 15 (2001) 1153–1166.
[32] G.T.S. Done, A. Simpson, Dynamic stability of certain conservative and non-conservative systems, *Institution of Mechanical Engineers-Journal of Mechanical Engineering Science* 19 (1977) 251–263.
[33] J. Horáček, I. Zolotarev, Influence of fixing the edges of a shell conveying fluid on its dynamic characteristics, *Soviet Applied Mechanics* 20 (1984) 756–765.
[34] M.P. Païdoussis, J.-P. Dennis, Flutter of thin cylindrical shells conveying fluid, *Journal of Sound and Vibration* 20 (1972) 9–26.
[35] L.K. Shayo, C.H. Ellen, Theoretical studies of internal flow-induced instabilities of cantilever pipes, *Journal of Sound and Vibration* 56 (1978) 463–474.